A Coaxial Noise Standard for the 1 GHz to 12.4 GHz Frequency Range

William C. Daywitt

Electromagnetic Fields Division
National Engineering Laboratory
National Bureau of Standards
U.S. Department of Commerce
Boulder, Colorado 80303

U.S. DEPARTMENT OF COMMERCE, Malcolm Baldrige, Secretary

NATIONAL BUREAU OF STANDARDS, Ernest Ambler, Director

Issued March 1984

National Bureau of Standards Technical Note 1074
Natl. Bur. Stand. (U.S.), Tech Note 1074, 44 pages (Mar. 1984)
CODEN: NBTNAE

U.S. GOVERNMENT PRINTING OFFICE
WASHINGTON: 1984

For sale by the Superintendent of Documents, U.S. Government Printing Office, Washington, DC 20402

CONTENTS

A Coaxial Noise Standard for the 1 GHz to 12.4 GHz Frequency Range

William C. Daywitt

Electromagnetic Fields Division
National Bureau of Standards
Boulder, Colorado 80303

This note describes the design and construction of a coaxial thermal noise standard. The standard is designed to operate at the boiling point of liquid nitrogen with a noise temperature accurate to ± 1 K in the frequency range from 1 GHz to 12.4 GHz.

Key words: coaxial; error analysis; microwave; noise standard.

1. Introduction and Description

The block diagram shown in figure 1 depicts two of the steps involved in calibrating the spectral power output [1] of a noise source by use of a noise standard and a noiseless radiometer, where the ratio R of the net spectral power p_x from the noise source under test to the net power p_a from the standard is measured by the radiometer. In terms of the reflection coefficients shown in the figure and the noise temperatures [1] T_x and T_s of the source under test and the standard,

$$R = \left(\frac{T_x}{T_s}\right)\left(\frac{1 - |\Gamma_x|^2}{1 - |\Gamma_s|^2}\right)\left|\frac{1 - \Gamma_r \Gamma_s}{1 - \Gamma_r \Gamma_x}\right|^2 . \qquad (1)$$

In the microwave and millimeter-wave calibration systems presently in use at the National Bureau of Standards (NBS) [2,3], only the magnitudes of the reflection coefficients are measured, and a determination of T_x from eq (1) is not exact since the corresponding phases must be known to calculate the last factor in the equation. Consequently, in addition to requiring low-reflection standards, the front ends of the present systems must be tuned to reduce Γ_r and the resulting errors associated with these unknown phases. However, a 6-port reflectometer [4] has been incorporated into a new, automated system

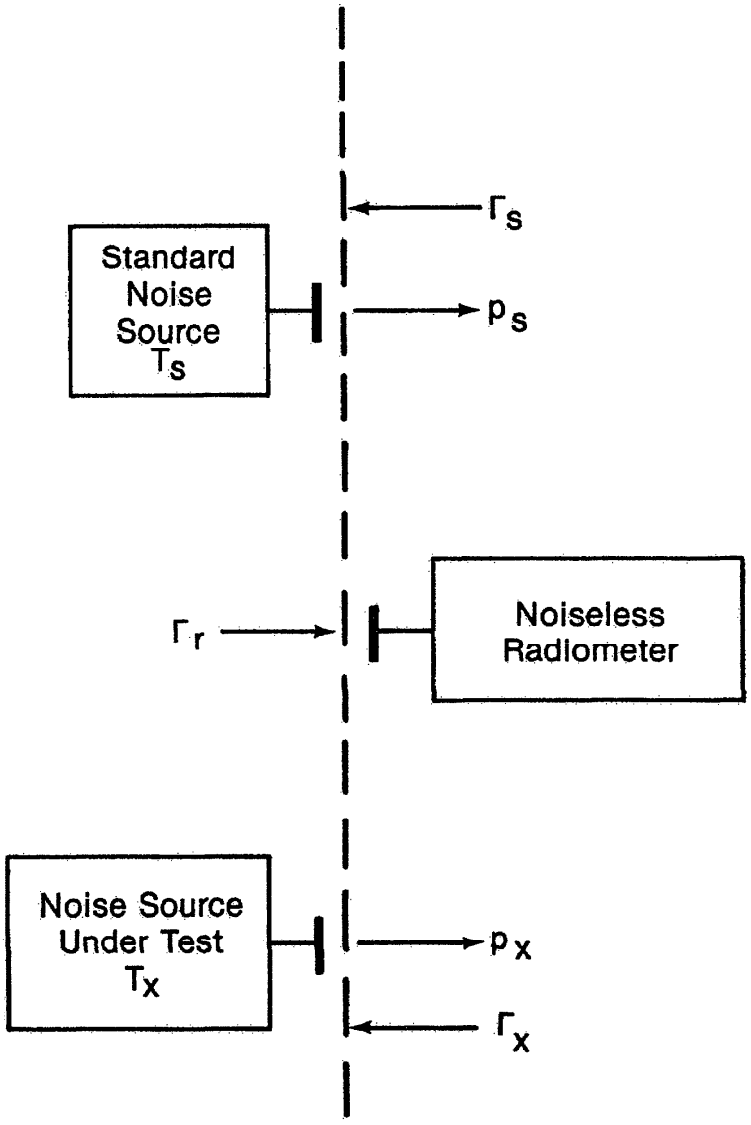

Figure 1. Block diagram for a noise calibration.

under development [5] for the frequency range from 2 GHz to 12 GHz, allowing the phases of the reflection coefficients to be measured in addition to their magnitudes. This capability obviates the need to tune the system front ends or the need to build broadband, reflectionless noise standards. A description of the design, construction, and calculation of the noise temperature for the standard to be used with this new system is presented in this note.

Although not reflectionless, the noise standard is nominally 50 Ω, and consists of a modified commercial termination immersed in a liquid-nitrogen bath. The termination is connected to a precision type N (male) connector at room temperature via a coaxial transmission line whose center conductor is supported by two low-loss beads. Two unique features are incorporated into the design: to eliminate the strain on the connector when the standard is attached to the radiometer, the termination and line have been loosely connected to the cryogenic bath; and the bead supports have been manufactured from a ceramic material of high thermal conductivity to positively lock the center conductor to specified temperatures at the bead positions, eliminating significant heat flow into the termination and condensation on the center conductor of the output connector. Figure 2 shows an assembly drawing of the standard and a subassembly drawing of the termination, center, and outer conductors. Figure 3 is a photograph of the assembled standard. The line and termination (items 1, 4, and 6 in figure 2) are fixed to a set of legs (3) that rest on, but which are not attached to, the cover (15) of the enclosure (27) housing a vacuum Dewar (25A). The line and termination are thus free to move within the confines of the heating ring (9A) through which water is circulated to maintain the enclosure cover (15) at room temperature. The upper, or room-termperature, bead (34) and line are maintained at room temperature by circulating water through the housing (1B) attached to the upper part of the line. The environment of the stainless steel, temperature-transition portion (4) of the line is kept at a reduced temperature by the copper sleave (21), the height of which is adjusted by rotating it with respect to the lower barrel (22). This barrel rests on a funnel (25B) which, by adjusting the legs (23), permit the entire section (21 and 22) to be centered in the Dewar. The funnel collects boil-off gas and directs it to the bubble collector (38) which forces the gas up past the lower, fan-shaped bead (35) into the cavity between the center and outer conductors of the

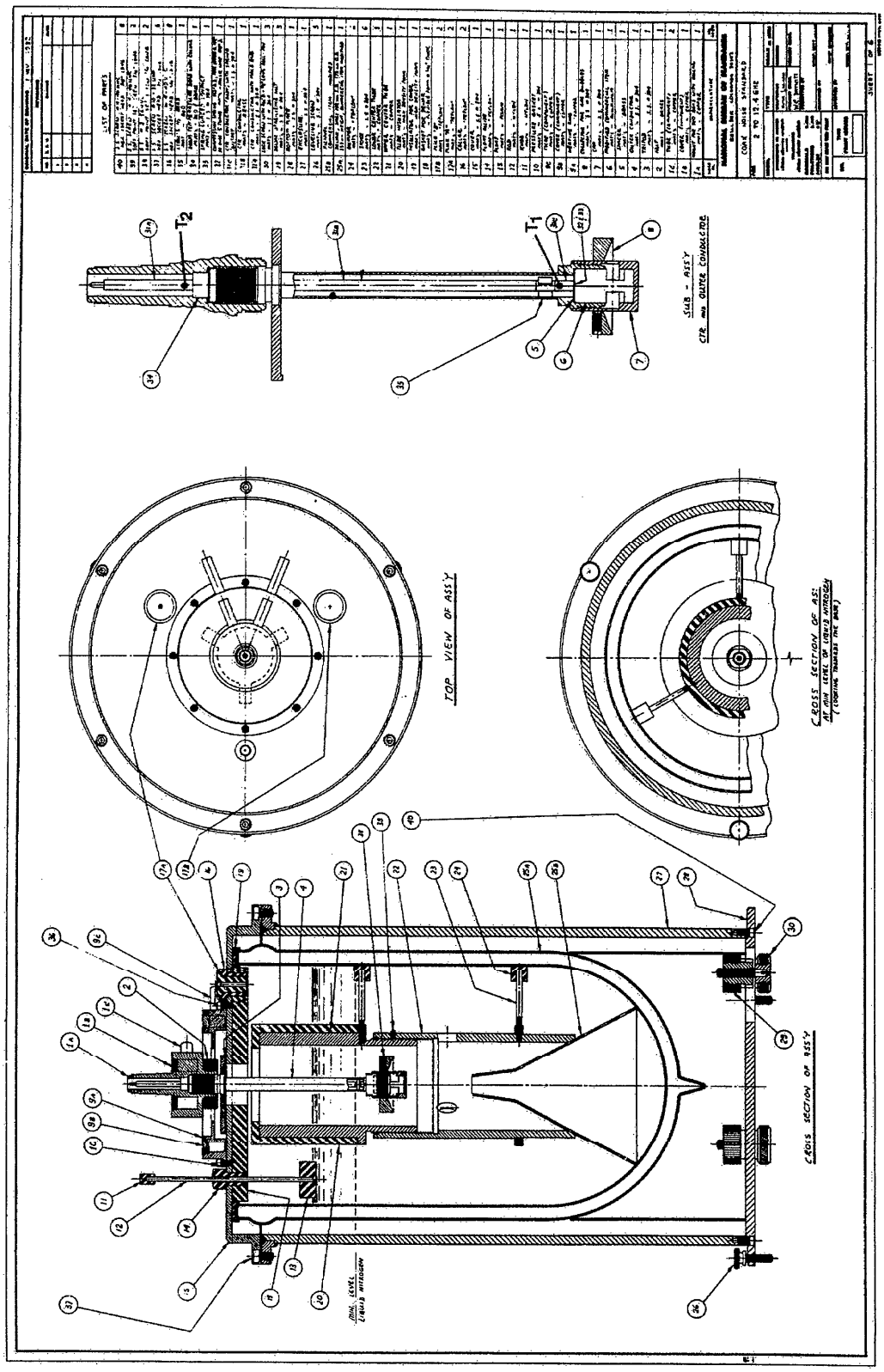

Figure 2. Assembly drawing of the noise standard.

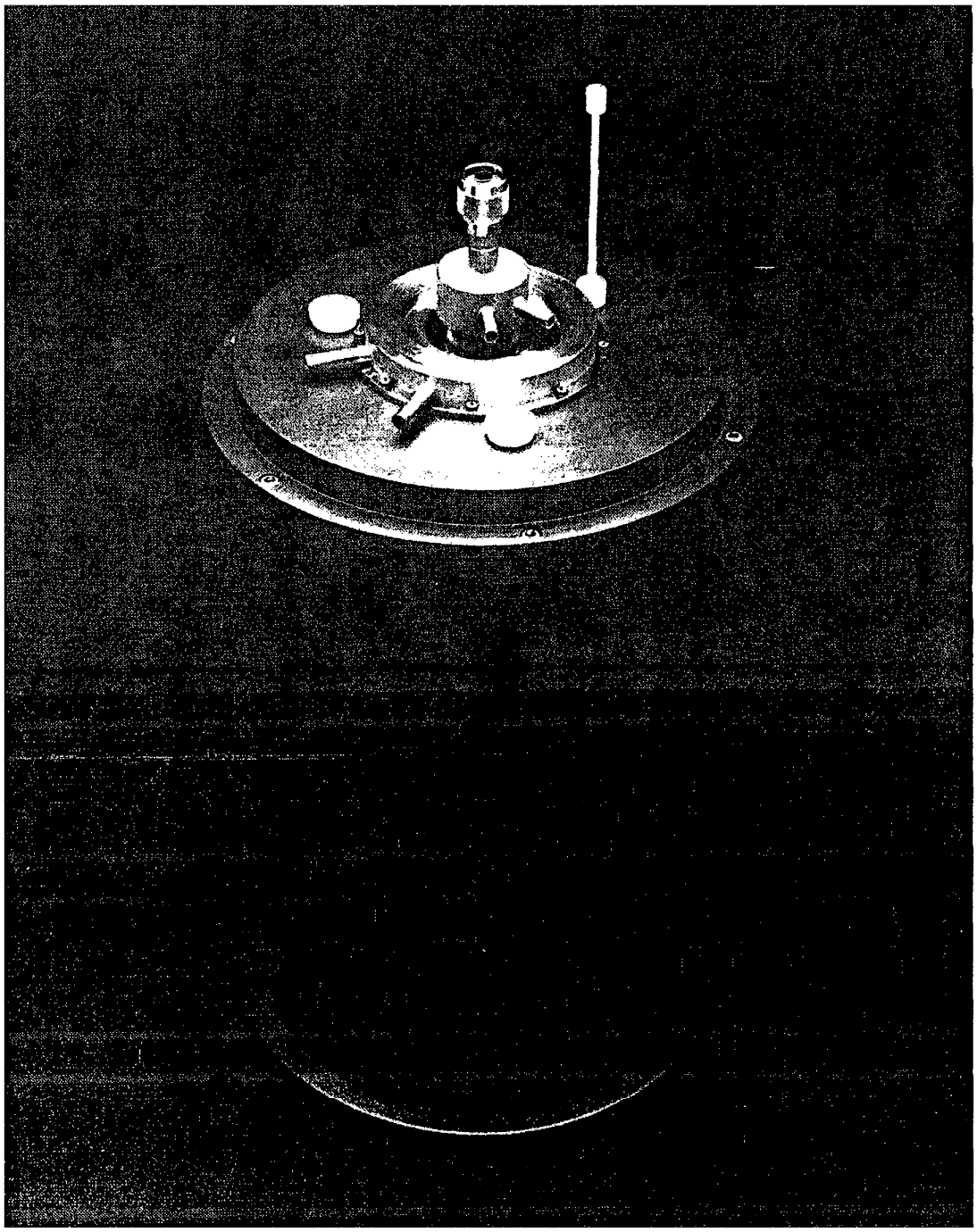

Figure 3. Photograph of the assembled standard.

temperature-transition part of the line. The lower part of the terminating element (6) below the bubble collector remains bathed in the liquid nitrogen. Keeping the liquid out of the transition region and away from the top of the terminating element considerably reduces the reflection from these regions that would otherwise be present. The standard is usable, and the noise-temperature output equation described in the next section is valid, when the liquid-nitrogen level resides between the top of the Dewar and the minimum level shown in the drawing, the boil-off time between these levels being approximately 5 hours.

A large number of possible bead materials were considered, the primary requirements being a relatively low dielectric constant (6 or less), a low loss tangent (0.001 or less), and a relatively high thermal conductivity. The most suitable materials satisfying the first two requirements were cross-linked polystyrene, fused silica, and the ceramic beryllium oxide. The thermal conductivities of these materials is shown in table 1 along with those of copper and nitrogen gas [6,7]. The most striking feature of the table is the high thermal conductivity of beryllium oxide, which even exceeds that of copper in between the temperatures shown. The effect of these various conductivities on the temperature of the center conductor is illustrated by estimating the temperature T_2 of the center conductor at the connector and the temperature T_1 just below the liquid-nitrogen bead (see figure 2). The estimates are shown in the last two columns of table 1. Since the temperature (271 K) of the line above an upper polystyrene bead is less than the dew point (282 K) in the laboratory, this material was immediately eliminated from consideration. With a fused silica bead, the temperature (85 K) below the lower bead is 9 K greater than the boiling temperature of the liquid and the base of the terminating element. Thus, there will be a 9 K temperature gradient from that point to the base of the element, causing a significant error in estimating the noise temperature of the standard. Berylllium oxide was chosen to eliminate this gradient. Although otherwise very tough and stable, one drawback from using beryllium oxide is that the dust generated while grinding the material is toxic [8], with the resulting inconvenience of having the beads manufactured in a grinding shop that handles this type of material. The equations used to design the beads are found in Appendix A.

Table 1. The thermal conductivity of various materials at 76 K and 297 K

Material	Thermal conductivity (W/cm/K) at 76 K	297 K	T_1(K)	T_2(K)
Copper	6	4	---	---
Beryllium oxide	3	2	76.08	296.96
Fused silica	0.008	0.01	85	292
Cross-linked polystyrene	0.001	0.001	94	271
Nitrogen gas	0.0001	0.0004	---	---

The stainless-steel center and outer conductors were gold plated to reduce their dissipative losses, and thereby increase the accuracy of the calculated noise temperature of the standard. The plating thickness was determined from an equation derived in Appendix B giving the relative error in the attenuation coefficient versus depth of plating.

2. Noise Temperature and Errors

An expression for the noise temperature of the standard is derived in Appendix C, and takes the approximate form

$$T_s \triangleq \varsigma(T_m + \Delta T) \tag{2}$$

where ς is the approximate quantum mechanical correctio discussed at the end of appendix C, T_m is the temperature of the terminatic , and ΔT is a correction noise temperature arising from excess noise contributed to the output by dissipative losses in the transmission line and room-temperature bead. From Appendix C

$$\Delta T = 2.64 \times 10^{-3} f^{1/2} |\Gamma_s|^2 (T_a - T_m) + [0.611 - 2.55 \times 10^{-3} (T_m - 76)$$

$$+ 3.82 \times 10^{-3} (T_a - 297)] (0.6 f^{1/2} + 0.011 f)/0.611 \tag{3}$$

where T_a is the temperature (kelvins) of the water flowing around the upper bead and line and is close to room temperature; Γ_s is the measured reflection coefficient of the standard; and f is the measurement frequency in GHz. T_m is calculated (± 0.01 K) from the atmospheric pressure P via the vapor pressure equation [9] ($T_m = T + 0.04$, where the 0.04 is due to the average hydrostatic pressure of the liquid above the termination)

$$\ell nP = N_1/T + N_2 + N_3 T + N_4 (T_c - T)^{1.95} + N_5 T^3$$

$$+ N_6 T^4 + N_7 T^5 + N_8 T^6 + N_9 \ell nT \tag{4}$$

where the pressure is expressed in atmospheres, T is in kelvins, and where T_c is the critical temperature (126.20 K). The coefficients are given in table 2, while a convenient table of the results with the pressure in millimeters of mercury is given in table 3. The first term in eq (3) involving the reflection coefficient is a correction due to that noise generated by the portion of the transmission line physically above the room-temperature bead which is propagated downward and reflected back by the combined reflection of the two beads and the termination. The upper curve in figure 13 is a plot of eq (3) with $\Gamma_s = 0$, $T_m = 76$ K, and $T_a = 297$ K.

Table 2. Coefficients for the nitrogen vapor-pressure equation [9]*

Coefficient	Numerical value	Coefficient	Numerical value
N_1	$0.8394409444 \times 10^{4}$	N_6	$-0.5944544662 \times 10^{-5}$
N_2	$-0.1890045259 \times 10^{4}$	N_7	$0.2715433932 \times 10^{-7}$
N_3	$-0.7282229165 \times 10^{1}$	N_8	$-0.4879535904 \times 10^{-10}$
N_4	$0.1022850966 \times 10^{-1}$	N_9	$0.5095360824 \times 10^{3}$
N_5	$0.5556063825 \times 10^{-3}$		

*Coefficients are for temperature in kelvin and pressure in atmospheres.

Seven sources of error in using eqs (2) and (3) to calculate the noise temperature arise from: uncertainties in T_m, T_a, and the dc resistivity of the conductor walls; uncertainty in the temperature distribution of the conductors between the two beads; surface roughness of the conductor walls; uncertainty in the loss tangent for the room-temperature bead; reflections by the termination and the beads. The error due to T_m is a result of: uncertainties (± 0.01 K) in the vapor-pressure eq (4); uncertainty (± 1 mm Hg) in

determining the atmospheric pressure; variation (± 3 cm) in the liquid-nitrogen head about its average level above the termination; and an uncertainty in the noise output of the terminating element due to a slight temperature gradient (0.1 K) across its surface. The resulting noise-temperature error (+ 0.21%, - 0.07%) is displayed along with the uncertainties in the sources of the error under item 1 in table 4. The uncertainty (± 1 K) in the water temperature resulting in a ± 0.02% error in the noise temperature is displayed as item 2.

Table 3. Liquid-nitrogen boiling temperature in kelvins versus pressure in millimeters of mercury

Pressure mm of mercury	Temperature in kelvins									
	0	1	2	3	4	5	6	7	8	9
610	75.53	75.54	75.56	75.57	75.58	75.60	75.61	75.62	75.63	75.65
620	75.66	75.67	75.69	75.70	75.71	75.73	75.74	75.75	75.76	75.78
630	75.79	75.80	75.82	75.83	75.84	75.85	75.87	75.88	75.89	75.91
640	75.92	75.93	75.94	75.96	75.97	75.98	75.99	76.01	76.02	76.03
650	76.04	76.06	76.07	76.08	76.09	76.11	76.12	76.13	76.14	76.16
660	76.17	76.18	76.19	76.21	76.22	76.23	76.24	76.26	76.27	76.28
670	76.29	76.31	76.32	76.33	76.34	76.35	76.37	76.38	76.39	76.40
680	76.42	76.43	76.44	76.45	76.46	76.18	76.49	76.50	76.51	76.52
690	76.54	76.55	76.56	76.57	76.58	76.60	76.61	76.62	76.63	76.64
700	76.66	76.67	76.68	76.69	76.70	76.72	76.73	76.74	76.75	76.76
710	76.77	76.79	76.80	76.81	76.82	76.83	76.84	76.86	76.87	76.88
720	76.89	76.90	76.91	76.93	76.94	76.95	76.96	76.97	76.98	77.00
730	77.01	77.02	77.03	77.04	77.05	77.06	77.08	77.09	77.10	77.11
740	77.12	77.13	77.14	77.16	77.17	77.18	77.19	77.20	77.21	77.22
750	77.23	77.25	77.26	77.27	77.28	77.29	77.30	77.31	77.32	77.34
760	77.35	77.36	77.37	77.38	77.39	77.10	77.41	77.42	77.44	77.45
770	77.46	77.47	77.48	77.49	77.50	77.51	77.52	77.54	77.55	77.56

Table 4. Noise temperature error components (1 GHz to 12.4 GHz)

	Source error	Magnitude	% error in T_s
1.	T_m	---	$^{+\ 0.21}_{-\ 0.07}$
	V-P equation	± 0.01 K	---
	Pressure	± 1 mm Hg	---
	Head	± 3 cm	---
	Gradient	+ 0.1 K	---
2.	T_a	± 1 K	± 0.02
3.	ρ	---	$\left(^{+\ 0.06}_{-\ 0.026}\right) f^{1/2}$
	dc value	± 5%	---
	Plating depth	± 6.6%	---
4.	Surface roughness	+ 2%	+ 0.01 $f^{1/2}$
5.	Loss tangent	± 10%	± 0.0036 f
6.	Temperature distribution	---	± 0.078 $f^{1/2}$
7.	Internal reflections	< 0.1	$\left[\left(^{+\ 0.045}_{-\ 0.014}\right) \pm 0.054\ |r_s|\right] f^{1/2}$
	Total error (linear sum)	$\left(^{+\ 0.23}_{-\ 0.09}\right) + \left[\left(^{+\ 0.19}_{-\ 0.12}\right) \pm 0.05\ |r_s|\right] f^{1/2}$	± 0.0036 f

An uncertainty of ± 5% is assumed for the resistivity, where the error due to an insufficient depth of gold plating is included. This latter uncertainty arises because the attenuation coefficient of the line is calculated

assuming solid gold conductors. The resulting uncertainty is estimated in Appendix B to be ± 6.6%, and combined in the resistivity error leads to the noise-temperature error shown under item 3 in the table.

Since the surface of the conductors are not perfectly smooth, there is a greater surface area available to absorb the energy traveling down the transmission line than that assumed for an ideally smooth surface. The effect of this surface roughness is not great in the microwave frequency region [10], and is assumed in the present case to cause an attenuation increase of less than 2%.

The attenuation in the room-temperature bead support is calculated from the measured loss tangent of the beryllium oxide bead material. The measurement uncertainty is estimated to be no greater than ± 10% of the loss tangent, and results in the noise-temperature error shown under item 5.

As the liquid-nitrogen level in the standard drops (due to boil off) from near the top of the Dewar to the minimum point shown in figure 2, the temperature gradient along the inner and outer conductors vary, causing a change in the excess noise from that portion of the line between the two bead supports. Therefore, since the corresponding noise temperature is calculated (see eq (C2)) for the average gradient, an error results. The magnitude of the error is shown under item 6.

Internal reflections due to the two beads and the termination also result in an error in the calculated noise temperature. By keeping the reflection coefficient magnitude of the lower bead and termination, and each of the two upper bead faces below a 0.1, it is possible to keep the resulting noise-temperature error less than the amount shown in the table under internal reflections.

The total error is defined as the linear sum of the right-hand column in table 4, and is reproduced in graphical form in figure 4. For example, the systematic error at 10 GHz for a total 0.3 reflection coefficient is + 0.91% and - 0.56% of the calculated noise temperature.

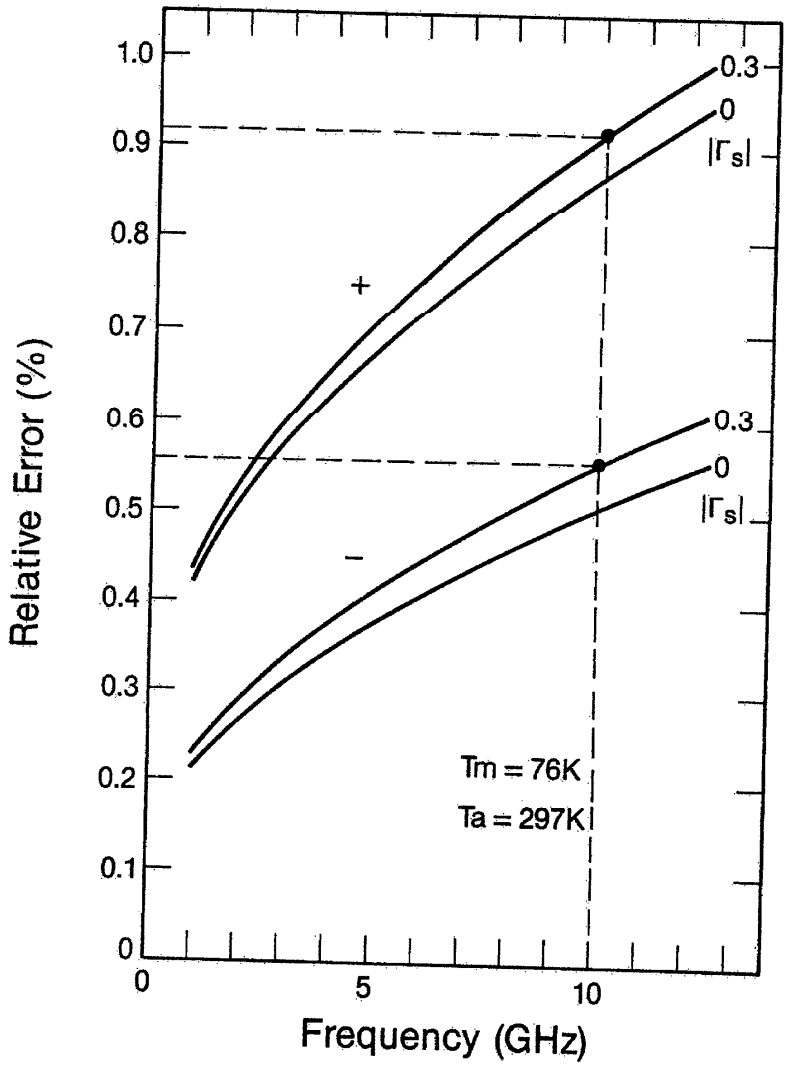

Figure 4. Relative noise temperature error versus frequency.

3. Conclusions

A cryogenic noise standard (fig. 3) has been described whose noise temperature is calculable to an error less than ± 1% in the frequency range from 1 GHz to 12.4 GHz.

Dielectric constant/loss tangent measurements have been performed (fig. 5) for the ceramic material beryllium oxide in the temperature range from 100 K to 300 K that had previously been unavailable, and an equation was derived (Appendix B) to estimate the plating depth for a required accuracy in calculating the attenuation coefficient for a wave constrained to propagate along a metallic surface.

4. Acknowledgments

The author gratefully acknowledges the support of the following individuals and organizations: Drs. Howard Bussey and Robert Beatty for making some unpublished work on calculating TE_{11} bead resonances available; Dr. Bussey for providing a computer program (and some patient coaching) and a silver cavity for determining the dielectric properties of the beryllium oxide; Dan Briggs of the Coors Spectro-Chemical Laboratory for performing the dielectric measurements; Mike Kuettner of the NBS shops for some very fine machining; Newark Air Force Station for support in manufacturing the standard; and the Calibration Coordination Group of the Defense Department for support of some early (1972-73), preliminary investigations.

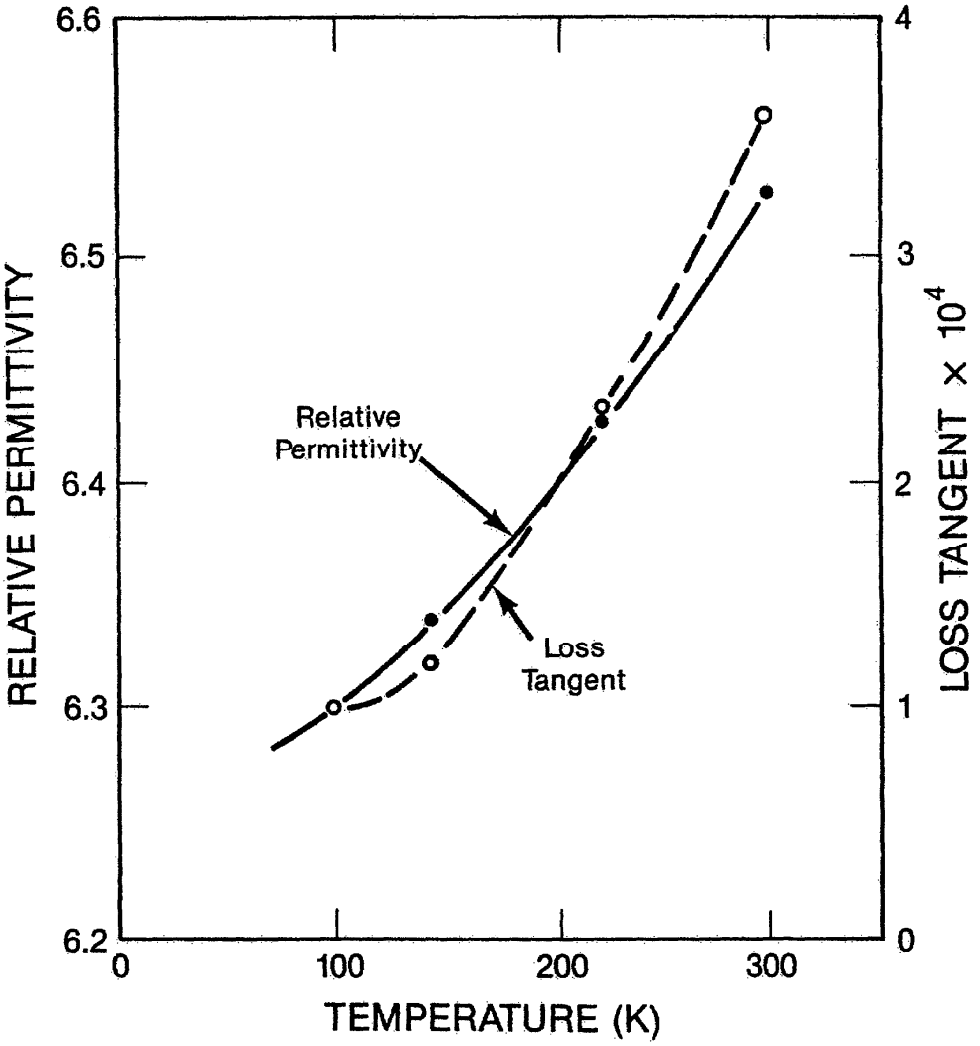

Figure 5. Dielectric properties of BeO versus temperature at 9.3 GHz.

5. References

[1] IEEE Standard Dictionary of Electrical and Electronic Terms. New York, N. Y.: Wiley-Interscience, a division of John Wiley and Sons, Inc.; 1972.

[2] Wells, J. S.; Daywitt, W. C.; Miller, C. K. S. Measurement of effective noise temperature of microwave noise sources. IEEE Trans. on I & M, IM-3: 17-28; 1964 March.

[3] Daywitt, W. C. A reference noise standard for millimeter waves. IEEE Trans. on MT & T, MTT-21, No. 12: 845-847; 1973 December.

[4] Engen, G. F. An improved circuit for implementing the six-port technique of microwave measurements. IEEE Trans. on MT & T, MTT-25, No. 12: 1080-1083; 1977 December.

[5] Counas, G. J. 2.0 GHz to 4.0 GHz automated radiometer -- operation and service manual. Nat. Bur. Stand. (U.S.) NBSIR 83-1697; 1984 January.

[6] Childs, G. E.; Ericks L. J.; Powell, R. L. Thermal conductivity of solids at room temperature and below. Nat. Bur. Stand. (U.S.) Monogr. 131; 1973 September.

[7] Rose-Innes, A. C. Low temperature techniques. D. Van Norstrand Company, Inc.; 1964.

[8] Ferreira, L. E. Recommended practices for safe handling of beryllium oxide ceramics. Symposium on materials and electron device processing, Special Technical Publication No. 300, American Society for Testing and Materials: 145-155; 1961.

[9] Jacobsen, R. T.; Stewart, R. B.; McCarty, R. D.; Hanley, H. J. M. Thermophysical properties of nitrogen from the fusion line to 3500 R (1944 K) for pressures to 150,000 PSIA (10342 x 10^5 N/M^2). Nat. Bur. Stand. (U.S.) Tech. Note 648; 1973 December.

[10] Allison, J.; Benson, F. A. Surface roughness and attenuation of precision-drawn, chemically polished, electropolished, electroplated, and electroformed waveguides. Proc. IEEE, 102B: 251-259; 1955 March.

[11] Moreno, T. Microwave transmission design data. New York, N.Y.: Dover Publications; 1958.

[12] Cruz, J. E. Experimental verification of an equation for determining the effective dielectric constant of center conductor supports in coaxial transmission lines. Nat. Bur. Stand. (U.S.) Report 9195; 1966 March.

[13] Daywitt, W. C. A broadband coaxial noise source -- preliminary investigation. Nat. Bur. Stand. (U.S.) NBSIR 73-334; 1973 October.

[14] Bussey, H. E.; Beatty, R. W. Higher mode resonances of dielectric support beads in coaxial lines. Private communication.

[15] Jackson, J. D. Classical electrodynamics. New York, London: John Wiley and Sons, Inc.; 1962.

[16] Miller, C. K. S.; Daywitt, W. C.; Arthur, M. C. Noise standards, measurements, and receiver noise definitions. Proc. IEEE, Vol. 55, No. 6: 865-877; 1967 June.

[17] Ragan, G. L., ed. Microwave transmission circuits. Radiation Laboratory Series, Vol. 9; 1948.

Appendix A: Bead Support Design Equations

The equations collected in this appendix were used to design the two bead supports for the center conductor. The upper bead (fig. 2) is solid in cross section while the lower bead has a fan-shaped geometry to permit passage of boil-off gas up into the space between the center and outer conductors. Both were constructed from beryllium oxide whose dielectric properties were carefully measured at 9.3 GHz in the temperature range from 100 K to 300 K, the results of which are presented in figure 5. The relative dielectirc constants for designing the room-temperature (297 K) bead and the liquid-nitrogen (76 K) were determined from the figure to be 6.524 and 6.284, respectively.

Room-Temperature Bead

The diameter of the center conductor inside the bead was reduced to maintain a 50-Ω characteristic impedance via the equation [11]

$$\ell n\left(\frac{D_o}{D_i}\right) = 100\ \pi\ \epsilon_{re}^{1/2}\left(\frac{\epsilon_o}{\mu_o}\right)^{1/2} \tag{A1}$$

where D_o (0.7000 cm) is the inner diameter of the outer conductor, D_i is the reduced diameter of the center conductor, ϵ_{re} (6.375) is the effective dielectric constant of the bead with a slight gap between its inner diameter and the inner conductor diameter, and ϵ_o and μ_o are the free-space electric and magnetic permeabilities, respectively. The effective dielectric constant was calculated from the equation [12,13]

$$\epsilon_{re} = \frac{\ell n(b/a)}{\ell n(a_1/a) + \frac{1}{\epsilon_r}\ell n(a_2/a_1) + \frac{1}{\eta}\ell n(b_1/a_2) + \ell n(b/b_1)} \tag{A2}$$

where

$$\eta \equiv (1 - N\theta/2\pi) + (N\theta/2\pi)\epsilon_r\ . \tag{A3}$$

The parameters are defined in figure 6, where ϵ_r is the dielectric constant for the bad material (6.524 at room temperature). For the solid bead $N\theta$ is 2π, b_1 is the same as b (0.7 cm) since the bead was press fit into the outer

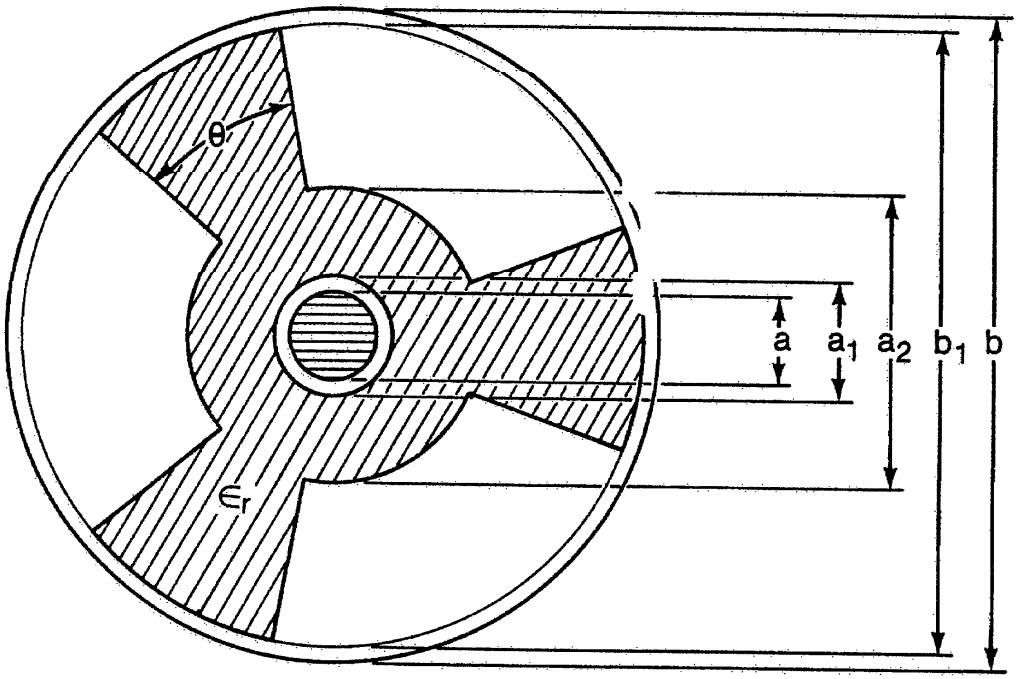

Figure 6. Geometry of a bead support.

conductor, and the inner diameter a_1 of the bead is 0.0008 cm larger than the inner-conductor diameter ($a \equiv D_i$) to allow for a slip fit. Equations (A1) and (A2) were solved for a_1 and ε_{re} to obtain 0.0861 cm and 6.375, respectively.

The maximum bead length is determined by the appearance of the first TE_{11} waveguide mode in the bead region for the operating frequency range of the standard. This length ℓ was determined from the equation [14]

$$\tan\left[\frac{2\pi}{\lambda}\left(\varepsilon_{re} - \lambda^2/\lambda_{cd}^2\right)^{1/2}\ell\right] = \left(\frac{\lambda^2/\lambda_{co}^2 - 1}{\varepsilon_{re} - \lambda^2/\lambda_{cd}^2}\right)^{1/2} \tag{A4}$$

where λ is the free-space wavelength corresponding to the maximum operating frequency (12.4 GHz), and λ_{co} and λ_{cd} are the cutoff wavelengths [11] for the TE_{11} mode in the bead region (with no bead material present) and the conductor region, respectively. For the room-temperature bead, the first root of this equation produced a length of 0.8 cm. The length of bead actually used was 0.45 cm.

The stray step capacitance at each end of the bead where the center-conductor diameter is reduced was eliminated (ideally) by removing some of the bead material in the immediate vicinity. The length d (cm) of material removed was calculated from [13]

$$d = \frac{1.5\ C\ (\varepsilon'_{re})^{1/2}}{1 - \varepsilon'_{re}/\varepsilon_{re}} \tag{A5}$$

where C is the step capacitance [11] with the dielectric removed (Morino's formula with his ε_r replaced by unity), and where the positions of the effective dielectric constants ε'_{re} and ε_{re} (both calculated from eq (A2) to be 2.022 and 6.375, respectively) are indicated in figure 7. The calculation produced a length of 0.0866 cm. Figure 8 shows a cutaway drawing of the bead where the previously discussed dimensions are collected.

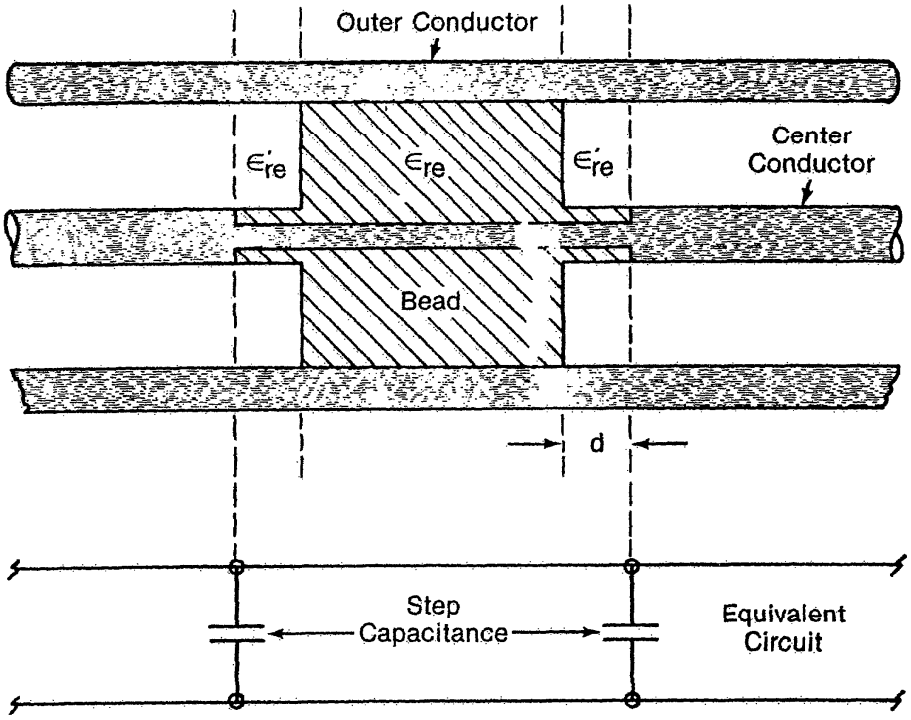

Figure 7. Equivalent circuit of a bead support.

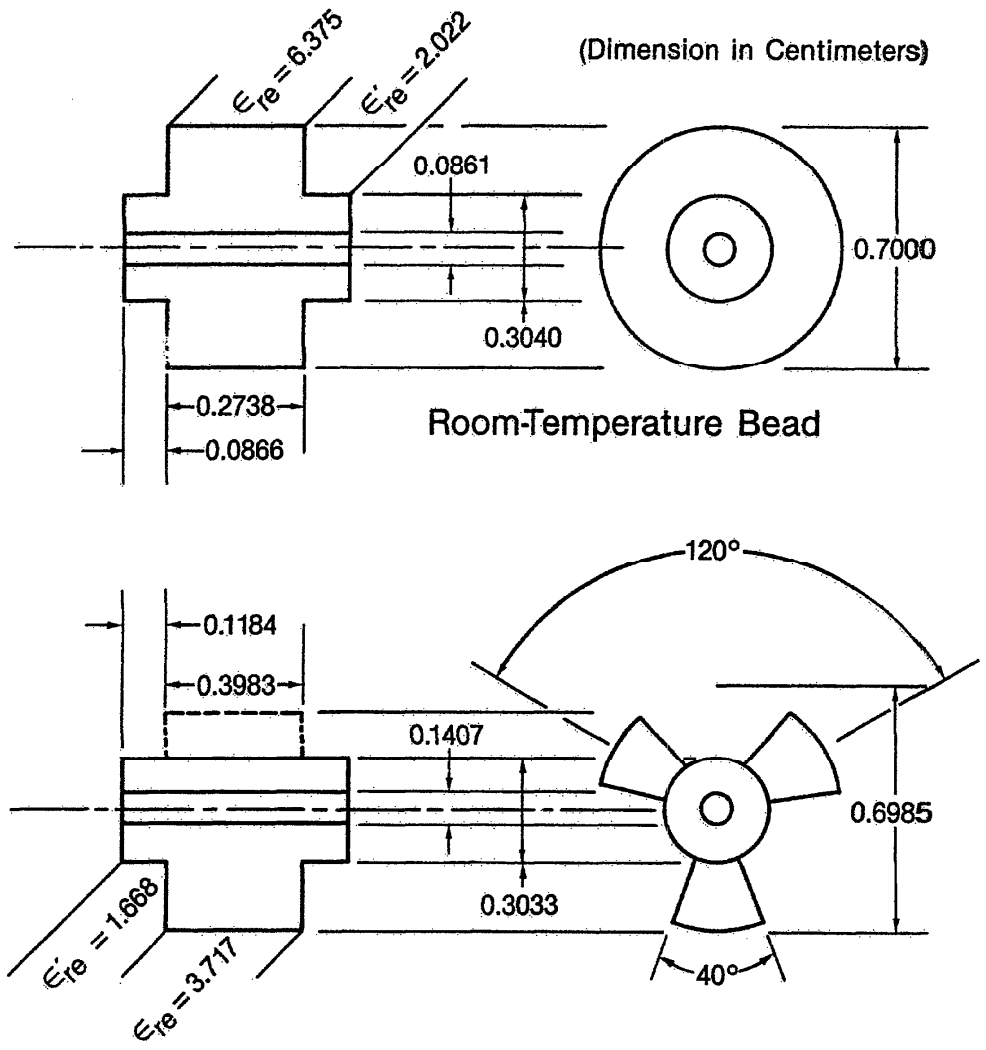

Figure 8. Dimensions for the room-temperature and liquid-nitrogen bead supports.

Liquid-Nitrogen Bead

The process just described was repeated for the lower, fan-shaped bead, with the results shown in figure 8.

Appendix B: Plating Depth

The conductors between the beads were constructed from stainless steel to reduce heat transfer into the cryogen and terminating element. To eliminate the corresponding increased loss caused by a lower electrical conductivity, the conductors were then plated with gold whose conductivity is some ten to 20 times that of stainless steel. Since the plating depth is relatively shallow, a portion of the fields propagating along the conductor penetrate through the gold and into the stainless steel. Thus, the loss will be greater than that calculated assuming solid gold conductors. The purpose of this appendix is to determine the resulting error as a function of the plating thickness.

Figure 9 shows a portion of a semi-infinite base metal (e.g., stainless steel) that has been plated with another metal to a thickness of ζ_1 to reduce the attenuation coefficient of the wave traveling along the surface. The magnetic field in free space that is parallel to the surface is denoted by $\underline{H}$, with $\underline{H}_1$ and $\underline{H}_2$ being the magnetic fields in the two metals that are induced by $\underline{H}$. To a first approximation [15], the fields in the metals obey the equations shown in the figure, where $\underline{n}$ is the unit normal to the surface and ζ is the inwardly-directed coordinate. The skin depths (MKS units) are given by ($i = 1,2$)

$$\delta_i = \left(\frac{2}{\mu_i \sigma_i \omega}\right)^{1/2} \tag{B1}$$

where μ_i and σ_i are the magnetic permeabilities and electrical conductivities, respectively, for the two metals, and ω is the radian frequency. The fields have the solutions (a harmonic time variation of $e^{-j\omega t}$ is assumed)

$$H_1 = A\, e^{(1-j)\zeta/\delta_1} + B\, e^{-(1-j)\zeta/\delta_1} \tag{B2}$$

$$H_2 = C\, e^{-(1-j)(\zeta-\zeta_1)/\delta_2} \tag{B3}$$

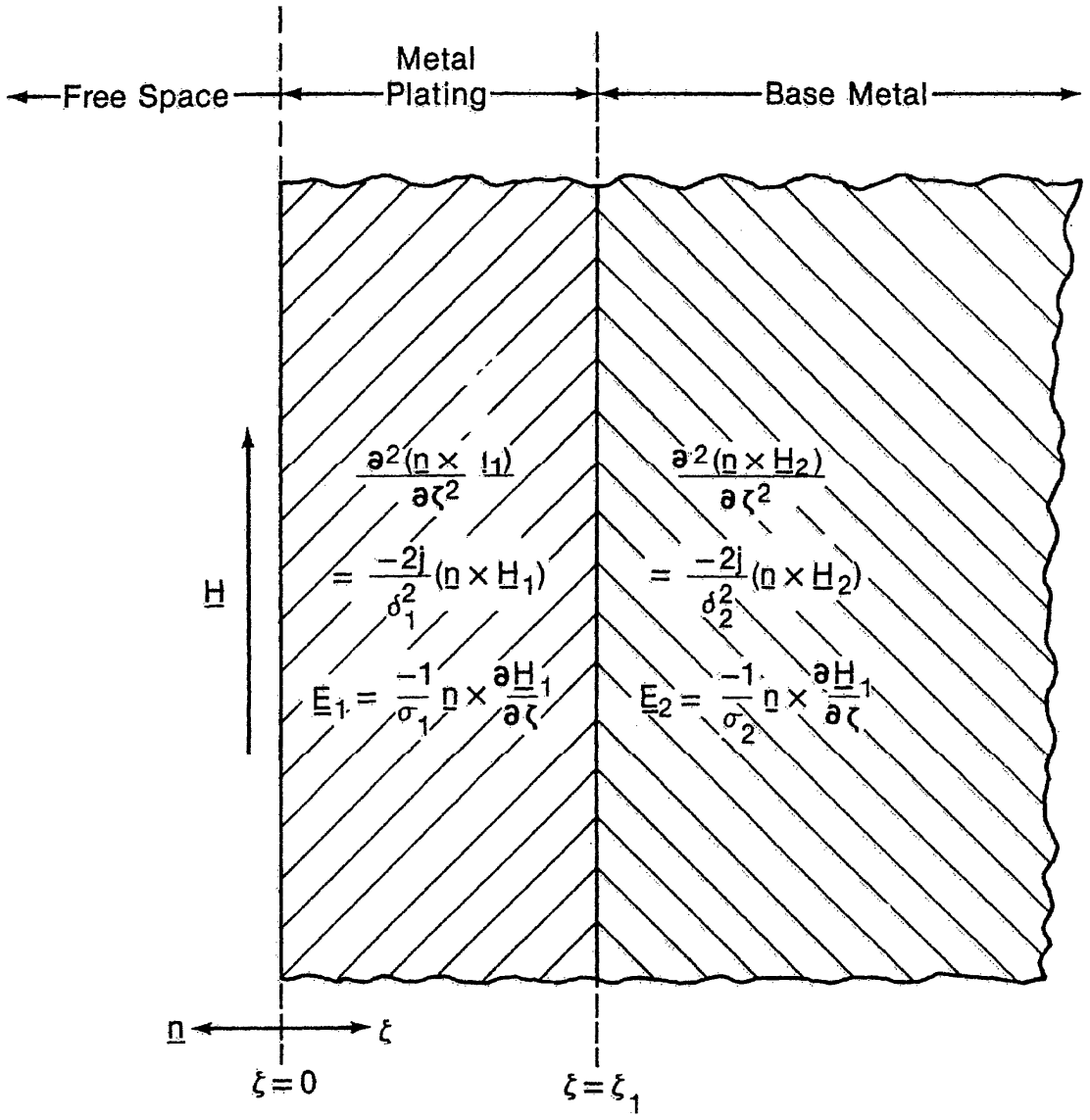

Figure 9. Schematic diagram of a plated conductor.

where the constants A, B, C are evaluated by satisfying the boundary conditions at the surfaces $\zeta = 0$ and $\zeta = \zeta_1$.

The power loss per unit area is calculated from

$$\frac{dP}{dA} = \frac{1}{2} \operatorname{Re} (\underline{n} \cdot \underline{E}_1 \times \underline{H}_1^*) \tag{B4}$$

at the $\zeta = 0$ surface which, after inserting the fields, reduces to the form

$$\frac{dP}{dA} = \left(\frac{dP}{dA}\right)_1 \operatorname{Re} \left\{ (1 - j) \left[\frac{1 + \left(\frac{r - 1}{r + 1}\right) e^{-2(1-j)\zeta_1/\delta_1}}{1 - \left(\frac{r - 1}{r + 1}\right) e^{-2(1-j)\zeta_1/\delta_1}} \right] \right\} \tag{B5}$$

where

$$r \equiv \left(\frac{\sigma_1}{\sigma_2}\right)^{1/2} . \tag{B6}$$

The first factor on the right of eq (B5) is the power loss assuming the plating thickness to be infinite. Thus, if the power loss is calculated assuming a finite thickness, the relative error ϵ is ($z \equiv \zeta_1/\delta_1$)

$$\epsilon \equiv \left| \operatorname{Re} \{(1 - j) [\ ]\} - 1 \right| \doteq 2\left(\frac{r - 1}{r + 1}\right) e^{-2z} \left| \cos 2z + \sin 2z \right| \tag{B7}$$

$$= 1.3\, e^{-2z} \left| \cos 2z + \sin 2z \right| . \tag{B7'}$$

The "1.3" factor is for gold plating (7.6×10^7 mhos) on 304 stainless steel (0.38×10^7 mhos) at 186 kelvin. Figure 10 shows a graph of eq (B7') which, for $z = 2$ (the plating thickness ratio used in the standard), indicates a 3.3% error in the calculation of the power loss.

It is convenient to include this error as an error in the resistivity, and, since the power loss is proportional to the square root of the resistivity, the relative error in the resistivity is 2ϵ or 6.6%.

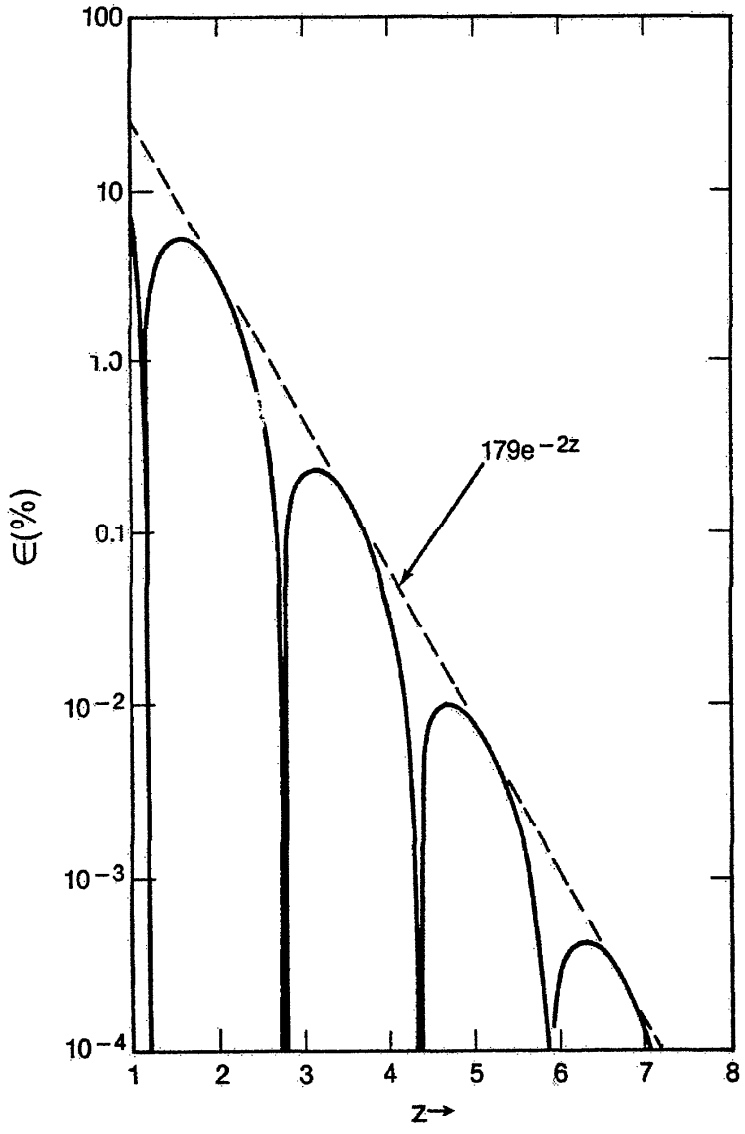

Figure 10. Relative power-loss error versus the ratio of plating depth to skin depth.

Appendix C: Noise Temperature Derivation

The essential features of the line and termination shown in figure 2 are depicted in figure 11a. The lower bead and termination are immersed in liquid nitrogen, while the upper bead and surrounding conductor are maintained at room temperature by circulating water. The inner and outer conductors have distinct temperature distributions which vary as the liquid nitrogen level varies, the inner (outer) conductor distribution being assumed to lie in the horizontally (vertically) cross-hatched region in figure 11b. Above (to the right in figure 11a) the room-temperature bead, both conductors are at room temperature T_a. Figure 11c is an electrical representation of the standard, where the lower bead and termination are lumped together in the impedance Z_g (with reflection coefficient Γ_g) since they are both at the same temperature. The compensation regions at the faces of the upper bead are represented by the T networks shown, while the portion of the bead between these regions is represented by a length of line. If the step capacitances at both faces were perfectly compensated, then both B_1 and B_2 would be infinite, leaving only the conductor and dielectric losses included in the resistances of the T networks. The line representing the bead between these networks includes both losses, also. The α's appearing in the figure represent noise efficiencies (available power ratios) [16], α_x [3] being the efficiency of the length of the temperature-transition portion of the line from point x to the bead at x_1. There is a separate T_x and α_x for the inner and outer conductor since the conductors generally have different temperature distributions.

The noise temperature is conveniently written in the form

$$T_s = T_m + \Delta T_1 + \ldots + \Delta T_5 \tag{C1}$$

where ΔT_1 through ΔT_5 represent the excess noise contributions from 0 to x_1, x_1 to x_2, x_2 to x_3, x_3 to x_4, and x_4 to x_5, respectively.

$$\Delta T_1 = \left[\int_0^{x_1} T'_x \, (1 - \alpha_x) \, dx\right] \alpha_2 \, \alpha_3 \, \alpha_4 \, \alpha_5 \tag{C2}$$

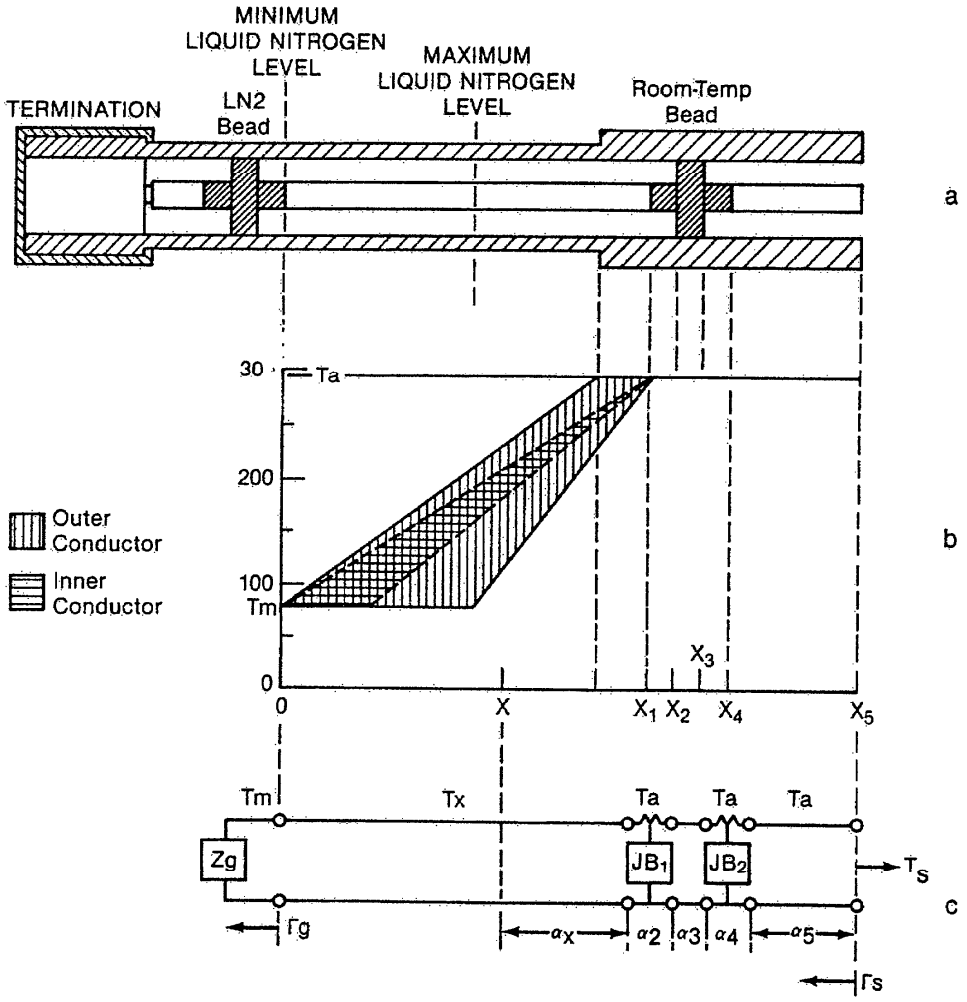

Figure 11. Schematic and electrical diagrams for estimating the noise temperature.

$$\Delta T_2 = (T_a - T_m)\ (1 - \alpha_2)\ \alpha_3\ \alpha_4\ \alpha_5 \tag{C3}$$

$$\Delta T_3 = (T_a - T_m)\ (1 - \alpha_3)\ \alpha_4\ \alpha_5 \tag{C4}$$

$$\Delta T_4 = (T_a - T_m)\ (1 - \alpha_4)\ \alpha_5 \tag{C5}$$

$$\Delta T_5 = (T_a - T_m)\ (1 - \alpha_5) \tag{C6}$$

where T_x' is the temperature gradient corresponding to T_x. The term in the bracket of eq (C2) represents the sum of two similar terms, one each for the inner and outer conductor, respectively. All of the noise efficiencies except α_5 were estimated under the assumption that there were no internal reflections, an approximation that leads to no significant error. After the preceeding equations were combined and reduced to a convenient nonintegral form by approximating the "exact" computer calculation shown in Appendix D, there resulted

$$\begin{aligned}\Delta T_1 + \ldots + \Delta T_5 = {} & 2.64 \times 10^{-3}\ (T_a - T_m)\ |\Gamma_s|^2\ f^{1/2} \\ & + [0.611 - 2.55 \times 10^{-3}\ (T_m - 76) \\ & + 3.82 \times 10^{-3}\ (T_a - 297)]\ (0.6\ f^{1/2} + 0.011\ f)/0.611\end{aligned} \tag{C7}$$

with an accompanying error of

$$[(^{+\ 0.045}_{-\ 0.014}) \pm 0.054\ |\Gamma_s|]\ f^{1/2} \tag{C8}$$

for the 1 GHz to 12.4 GHz frequency range. In evaluating eq (C2), the averages of the extreme limits of the shaded area in figure 11b were used for the inner and outer temperature distributions.

Attenuation coefficients for the various sections shown in figure 11c were evaluated according to the following equations: for the conductor losses [11]

$$a_i = \frac{1.44866 \times 10^{-4} \, (f \, \varepsilon_{re} \, \rho_i)^{1/2}}{D_i \, \ln (D_o/D_i)} \qquad (C9)$$

$$a_o = \frac{1.44866 \times 10^{-4} \, (f \, \varepsilon_{re} \, \rho_o)^{1/2}}{D_o \, \ln (D_o/D_i)} \qquad (C10)$$

where a_i and a_o are the attenuation coefficients (expressed in dB/cm) for the inner and outer conductors, respectively, f is the frequency in GHz, ε_{re} is the effective dielectric constant, ρ_i and ρ_o are resistivities in micro-ohm centimeters, and D_o and D_i are the outer and inner conductor diameters, respectively. ρ_o and ρ_i are different only when the temperatures of the outer and inner conductor are different. For dielectric losses, the attenuation coefficient is (dB/cm)

$$a = \frac{27.288 \, \varepsilon_r^{1/2} \tan\delta}{\lambda} \left[\frac{(\ln(D_1/D_i)) \, (\ln(D_o/D_i))^{1/2}}{(\ln(D_1/D_i) + \varepsilon_r \ln(D_o/D_1))^{3/2}} \right] \qquad (C11)$$

where ε_r is the dielectric constant of the material, tanδ is the loss tangent of the material, and λ is the free-space wavelength in centimeters. The remaining symbols in the equation are indicated in figure 12. The last equation was derived using a static approximation [17], and reduces to the equation given by Moreno [11] when the dielectric completely fills ($D_1 = D_o$) the space between the conductors.

The magnitudes of the various excess noise temperatures, eqs (C2) through (C6), are plotted as a function of frequency in figure 13 along with the total (ΔT) at the top of the figure. The dashed curves represent the effect of the error in (C8) on the calculation.

In the preceeding development, the temperatures T_m and T_a appearing explicitly in eqs (C1) through (C6) were, for convenience, assumed to be the thermodynamic or physical temperatures of the reservoir and transmission line,

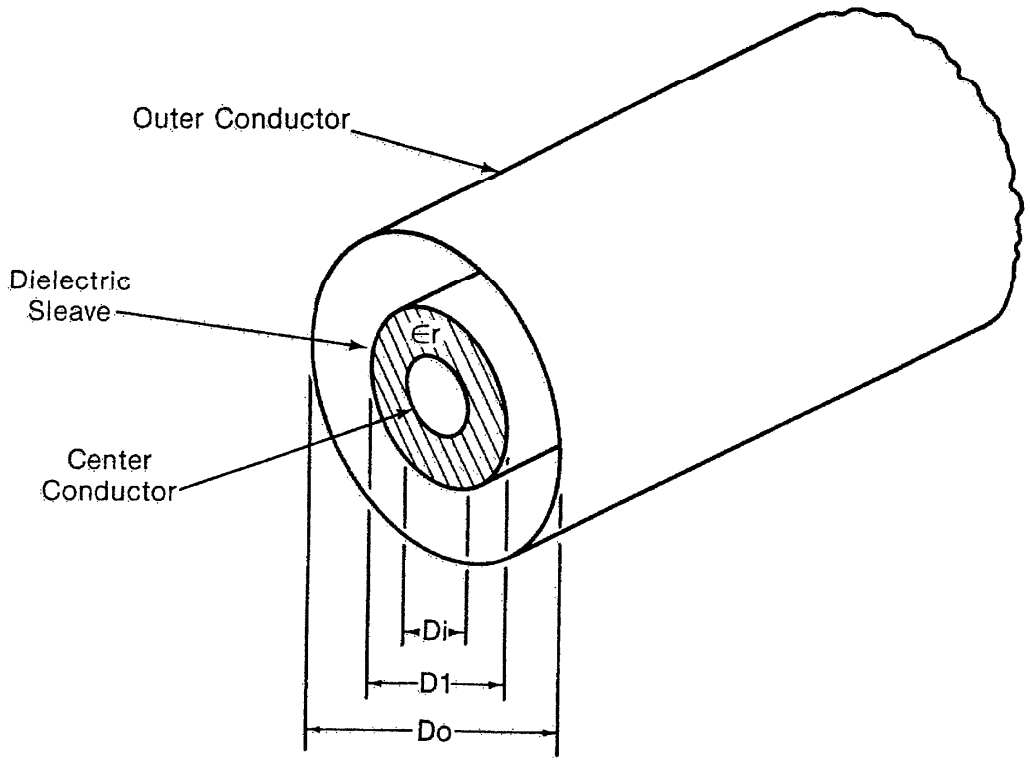

Figure 12. Schematic diagram of a center and outer conductor, and a dielectric sleave.

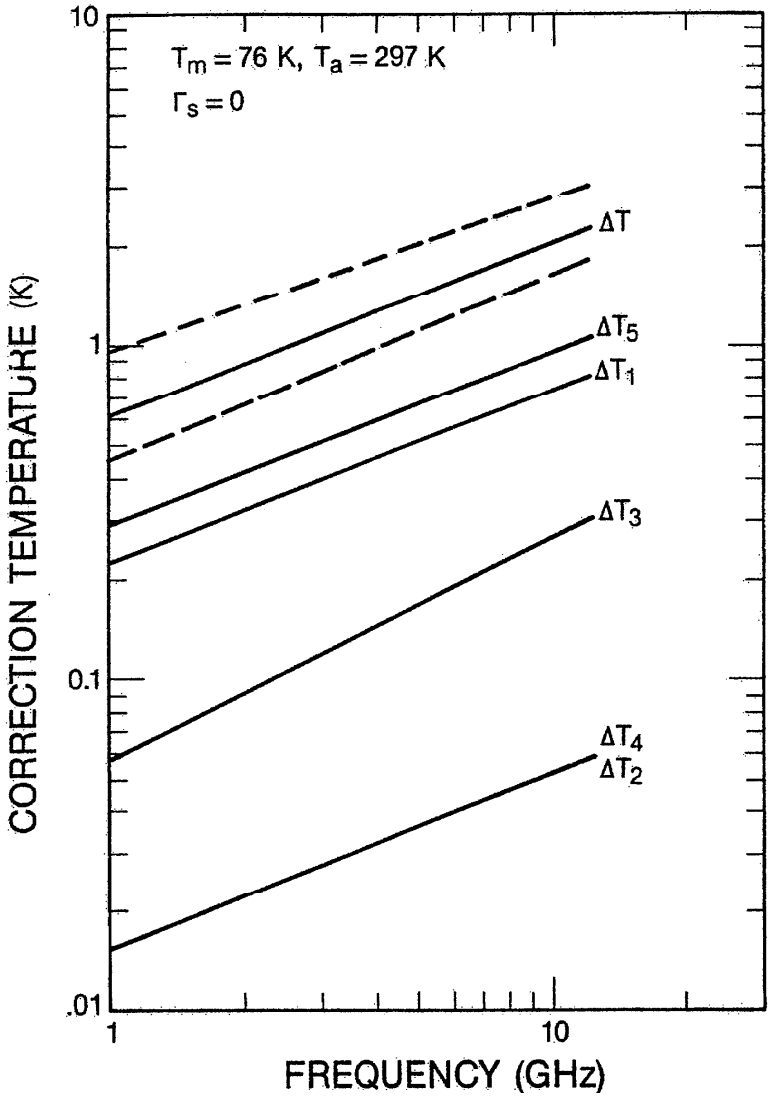

Figure 13. Various components of the noise temperature versus frequency.

respectively. To be exact, both of these temperatures should be replaced by their corresponding radiation temperatures, where the radiation temperature corresponding to a physical temperature T is calculated from the equation

$$(T)_{\text{radiation}} = \frac{hf/k}{e^{hf/kT} - 1} \tag{C12}$$

where h is Planck's constant, and k is Boltzmann's constant. An adequate approximation to eq (C1) for the 1 GHz to 12 GHz range where the thermodynamic temperatures are retained is given by

$$T_n \doteq \varsigma(T_m + \Delta T_1 + \ldots + \Delta T_5) \tag{C13}$$

where

$$\varsigma \equiv \frac{x}{e^x - 1} \tag{C14}$$

$$x \equiv \frac{hf}{kT_m} . \tag{C15}$$

Neglect of the correction factor ς in eq (C13) leads to an error varying from 0.06% to 0.4% in the frequency range under consideration.

Appendix D: Noise-Temperature Computer Code (Exact)

Following is a copy of the computer program used to perform an "exact" calculation of the noise temperature from which the approximation given by eq (C7) was derived.

```
 83/08/26. 13.27.52.
PROGRAM   TCX1

1 REM TCX1. NOISE TEMP FOR COAX
2 REM 9/10/82
4 DIM A(2000),B(2000),C(2000)
5 DIM V(100),W(100),X(2000),T(2000),U(2000)
7 GOSUB1000
9 GOSUB7000
10 GOSUB6000
20 GOSUB3000
48 PRINT
50 PRINT "L1,L2,L3"
52 PRINT "L1,T2,T3"
54 PRINT "D1,D2,D3,D4"
56 PRINT "ERE,EREP,L4,L5"
60 PRINT L1,L2,L3
62 PRINT G,T2,T3
64 PRINT D1,D2,D3,D4
66 PRINT E1,E2,L4,L5
69 PRINT
70 PRINT "A1(DB),DT1"
72 PRINT "A2L,A2D,A2S,DT2"
74 PRINT "A3L,A3D,DT3"
76 PRINT "A4L,A4D,A4S,DT4"
78 PRINT "A5,DT5"
80 PRINT -10*LGT(A1),H1
82 PRINT B1,B3,B2,H2
84 PRINT B4,B5,H3
86 PRINT B1,B3,B2,H4
88 PRINT -10*LGT(A5),H5
89 PRINT
90 PRINT "TM="T0,"TA="T3,"DT="H
99 PRINT
100 W5=T3-T0
102 W6=H/(T3-T0)
105 PRINT "TA-TM="W5,"(TN-TM)/(TA-TM)="W6
999STOP
1000 REM CONSTS
1005 N5=2000
1010 C0=1.44866E-4
1020 F=12.4
1030 D1=.304
1040 D2=.7
1060 C2=LOG(10)/10
1070 N6=N5-1
1080 D3=.08534
1082 D4=.7
1086 E1=6.375
1088 E2=2.022
1090 L4=.2738
```

```
1090 L4=.2738
1092 L5=.0866
1094 L2=L4+2*L5
1096 G=.000353
1098 L6=(D1-D3)/2
1099 D5=(D1+D3)/2
1110 L3=4.7
1499 RETURN
2000 REM RESISTVY CALC
2010 R=-.17+.008051*T
2099 RETURN
2100 REM ATTN AND EFF
2110 C1=C0*SQR(F)/LOG(D2/D1)
2130 FOR I1=1 TO N6
2140 T=(T(I1)+T(I1+1))/2
2150 GOSUB2000
2160 A(I1)=C1*SQR(R)/D1
2170 T=(U(I1)+U(I1+1))/2
2180 GOSUB2000
2190 B(I1)=C1*SQR(R)/D2
2200 NEXT I1
2210 Q1=X(N5)/N6
2220 Q2=(A(N6)+B(N6))*Q1/2
2222 C(N6)=1/10↑(Q2/10)
2229 N7=N5-2
2230 FOR I1=1 TO N7
2240 Q2=(A(N5-I1)+B(N5-I1))*Q1/2
2250 Q2=Q2+(A(N6-I1)+B(N6-I1))*Q1/2
2260 Q2=1/10↑(Q2/10)
2270 C(N6-I1)=C(N5-I1)*Q2
2280 NEXT I1
2290 A1=C(1)
2300 REM A2
2305 T=T2
2307 GOSUB2000
2310 C1=C0*SQR(F*R*E2)
2312 B1=C1*(1/D3+1/D4)*L5/LOG(D4/D3)
2314 B2=C1*L6/D5/LOG(D4/D5)
2316 B3=27.288*SQR(E1)*G*L5*F/29.9793
2318 B3=B3*LOG(D1/D3)*SQR(LOG(D4/D3))
2320 B3=B3/((LOG(D1/D3)+E1*LOG(D4/D1))↑1.5)
2324 A2=B1+B2+B3
2325 A2=1/10↑(A2/10)
2328 A4=A2
2330 REM A3
2332 C1=C0*SQR(F*R*E1)
2334 B4=C1*(1/D3+1/D4)*L4/LOG(D4/D3)
2336 B5=27.288*G*SQR(E1)*L4*F/29.9793
2338 A3=B4+B5
2340 A3=1/10↑(A3/10)
2350 REM A5
2352 T=T3
```

```
2352 T=T3
2354 GOSUB2000
2356 C1=C0*SQR(F*R)*L3
2358 A5=C1*(1/D1+1/D2)/LOG(D2/D1)
2360 A5=1/10^(A5/10)
2499 RETURN
3000 REM T.OUT
3005 GOSUB2100
3010 S3=0
3030 FOR I5=1 TO N6
3040 S3=S3+(T(I5)*A(I5)+U(I5)*B(I5))*C(I5)
3050 NEXT I5
3060 S3=S3*X(N5)/N6
3065 S3=C2*S3
3070 H1=S3*A2*A3*A4*A5
3072 H1=H1-T0*(1-A1)*A2*A3*A4*A5
3080 H2=(T2-T0)*(1-A2)*A3*A4*A5
3090 H3=(T2-T0)*(1-A3)*A4*A5
3100 H4=(T2-T0)*(1-A4)*A5
3110 H5=(T3-T0)*(1-A5)
3120 H=H1+H2+H3+H4+H5
3199 RETURN
6000 REM INPUT DATA READOUT
6010 RESTORE
6020 READ N9
6030 PRINT "FREQ="F
6032 PRINT
6070 PRINT "X","T"
6071 PRINT "      INNER"
6080 FOR I7=1 TO N9
6085 READ V,W
6090 PRINT V,W
6100 NEXT I7
6110 PRINT "      OUTER"
6118 READ N9
6120 FOR I7=1 TO N9
6130 READ V,W
6140 PRINT V,W
6150 NEXT I7
6299 RETURN
7000 REM DIST CALC
7005 RESTORE
7010 GOSUB7500
7020 Q=V(N9)/N6
7025 X(1)=0
7030 FOR J9=2 TO N5
7040 X(J9)=X(J9-1)+Q
7050 NEXT J9
7060 I8=2
7064 S9=(W(2)-W(1))/(V(2)-V(1)+1E-10)
7068 T(1)=W(1)
7070 FOR I9=2 TO N5
```

```
7070 FOR I9=2 TO N5
7080 IF X(I9)<V(I8) THEN 7090
7082 I8=I8+1
7083 IF X(I9)>V(I8) THEN 7082
7084 S9=(W(I8)-W(I8-1))/(V(I8)-V(I8-1)+1E-10)
7086 T(I9)=W(I8-1)+S9*(X(I9)-V(I8-1))
7088 GOTO7100
7090 T(I9)=T(I9-1)+S9*U
7092 T2=T(N5)
7094 T3=T2
7100 NEXT I9
7110 GOSUB7500
7120 I8=2
7130 S9=(W(2)-W(1))/(V(2)-V(1)+1E-10)
7140 U(1)=W(1)
7150 FOR I9=2 TO N5
7160 IF X(I9)<V(I8) THEN 7190
7162 I8=I8+1
7163 IF X(I9)>V(I8) THEN 7162
7164 S9=(W(I8)-W(I8-1))/(V(I8)-V(I8-1)+1E-10)
7166 U(I9)=W(I8-1)+S9*(X(I9)-V(I8-1))
7188 GOTO7200
7190 U(I9)=U(I9-1)+S9*U
7200 NEXT I9
7499 RETURN
7500 REM READER
7510 READ N9
7520 FOR J9=1 TO N9
7530 READ V(J9)
7540 READ W(J9)
7560 NEXT J9
7562 L1=V(N9)
7564 T0=W(1)
7599 RETURN
9000 REM DATA FORMAT: INNER THEN OUTER COND AS N,X1,Y1,...
9002 REM X1=0 & LAST X SAME FOR IN & OUT COND
9003 REM X'S IN CM
9010 DATA 3
9012 DATA 0,76,1.6,76
9014 DATA 10.6
9016 DATA 297
9100 DATA 4
9104 DATA 0,76,3.2,76
9106 DATA 10.1,297,10.6,297
9999 END
```

```
 83/08/26. 13.43.18.
PROGRAM   TCX1

FREQ= 12.4

X               T
     INNER
 0                76
 1.6              76
 10.6             297
     OUTER
 0                76
 3.2              76
 10.1             297
 10.6             297

L1,L2,L3
LT,T2,T3
D1,D2,D3,D4
ERE,EREP,L4,L5
 10.6             .447            4.7
 .000353          297.            297.
 .304             .7              .08534          .7
 6.375            2.022           .2738           .0866

A1(DB),DT1
A2L,A2D,A2S,DT2
A3L,A3D,DT3
A4L,A4D,A4S,DT4
A5,DT5
 3.19245E-2       .80176
 5.84851E-4       9.49576E-5      4.74420E-4      5.83582E-2
 3.28330E-3       2.75436E-3      .305519
 5.84851E-4       9.49576E-5      4.74420E-4      5.84549E-2
 2.02131E-2       1.0262

TM= 76           TA= 297.        DT= 2.25029

TA-TM= 221.     (TN-TM)/(TA-TM)= 1.01823E-2
```